Performance of an optical wireless communication system as a function of wavelength

Haim Manor and Shlomi Arnon

Optical wireless communication (OWC) is gaining acceptance in an increasing number of sectors of science and industry, owing to its unique combination of features: extremely high bandwidth, rapid deployment time, license- and tariff-free bandwidth allocation, and low power consumption, weight, and size. However, the major drawback of OWC in terrestrial applications is the threat of downtime caused by adverse weather conditions, such as fog and haze. Several researchers have proposed and developed communication systems that use far-IR radiation to mitigate weather effects. In this study we analyze the performance of a short-distance terrestrial OWC system as a function of wavelength. A mathematical model for OWC link performance is derived. Using this model, we perform a simulation of our system under different weather conditions. From the results of our calculations, the improvement of link availability for 10 μm compared with 0.785–1.55 μm for a distance of 1-km propagation is 0.2% (99.6–99.8%). This modest improvement should be considered relative to the complexity and cost of quantum cascade laser transmitters and far-IR receivers.

OCIS codes: 200.2610, 060.4510.

1. Introduction

Optical wireless communication (OWC) has become a practical high-bandwidth access tool. The schematic structure of a basic OWC system is shown in Fig. 1. At the transmitter, a laser beam is generated by an electric-to-optic process and is expanded and directed by a transmitting telescope. After propagation through the atmosphere, it is collected by a receiver telescope, optically filtered and concentrated onto the focal plane detector, and, finally, converted into an electric current by a reverse optic-to-electric process. The advantages of OWC are that (a) there are no licensing requirements (a time-saving feature); (b) no tariffs are required for its utilization (an operating cost saving); (c) there are no rf radiation hazards (eye-safe power levels are maintained); (d) there is no need to dig up roads; (e) it has a large bandwidth, which facilitates high data rates; (f) it is small, light, and compact; and (g) it has low power consumption. The main disadvantages of OWC systems are strict alignment requirements and adverse atmospheric weather-dependent effects.

Free-space optical communication has attracted considerable attention recently for a variety of applications.[1–3] Special attention has been paid to ways in which adverse weather conditions and background radiation affect transmission through the atmosphere.[4–6] As a result of these effects the performance of laser communication (lasercom) systems is extremely dependent on the laser's transmission wavelength.[7] Nowadays lasercom systems usually operate with well-established near-IR laser sources of 0.785-, 0.85, and 1.55-μm wavelengths.[8,9] However, previous studies based on available weather statistic measurements[10,11] indicated that weather effects can be mitigated by use of medium- and far-IR laser sources.[12–14] In that case, the new and versatile quantum cascade lasers (QCLs),[15] which are adjusted to operate within the atmospheric window regions in the mid-wave and long-wave IR (3–20-μm) wavelength band, can provide a solution to the atmospheric attenuation problem.[16–20] A comprehensive study of the effect of turbulence on communication links is described by Andrews and Phillips.[21] The effects of atmospheric turbulence and building sway on optical wireless communication systems are described in Ref. 22. Availability of free-space optics and hybrid free-space optics–rf systems in several cities worldwide is described in Ref. 9. In Refs. 8, 9, 23, and 24 the effects of fog and haze on the bit-error

The authors are with the Satellite and Wireless Communication Laboratory, Department of Electrical and Computer Engineering, Ben-Gurion University of the Negev, P.O. Box 653, IL-84105 Beer-Sheva, Israel. S. Arnon's e-mail address is shlomi@ee.bgu.ac.il.

Received 22 November 2002; revised manuscript received 11 April 2003.

0003-6935/03/214285-10$15.00/0

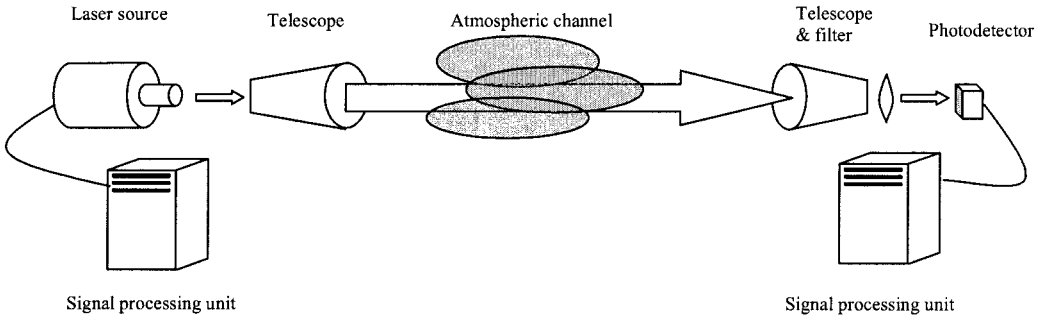

Fig. 1. Schematic structure of an OWC system.

rate of a free-space laser communication system are calculated and measured.

Here we analyze the wavelength dependence of lasercom system performance under several weather conditions for the purpose of making recommendations on preferable transmission wavelengths within the 0.4–20-μm band. The paper has the following outline: In Section 2 we describe the basic configuration of a general OWC system. In Section 3 we briefly review some special properties of QCL sources. A mathematical analysis is presented in Section IV, where we describe the optical signal–noise model and derive the signal-to-noise ratio link performance parameter. Detailed numerical results of our lasercom system simulation are given in Section 5. This simulation is performed for a specific set of circumstances under varied weather conditions based on hourly visibility observations that are available at most airports in the world. In Section 6 we draw our conclusions.

2. Free-Space Optical Wireless Communication System

There are three key functional elements of a free-space OWC system (see Fig. 2): the transmitter, the atmospheric channel, and the receiver. The transmitter converts the electronic signal into light. The light propagates through the atmosphere to the receiver, which converts the light back into an electronic signal. The transmitter includes a modulator, a laser driver, a LED or laser, and a telescope. The modulator converts bits of information into signals in accordance with the chosen modulation method. The driver provides the power for the laser and stabilizes its performance; it also neutralizes such effects as temperature and aging of the laser or LED. The light source converts the electrical signal into optic radiation. The telescope aligns the laser–LED radiation to a collimated beam and directs it to the receiver.

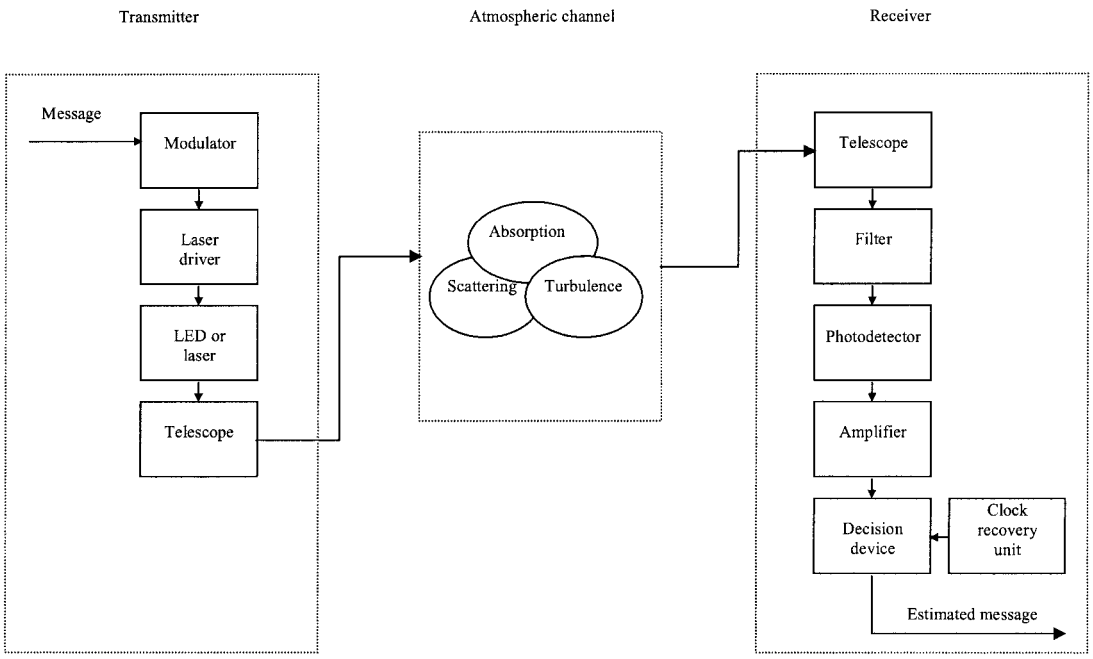

Fig. 2. Block diagram of an OWC system.

In the atmospheric channel, the signal is attenuated and blurred as a result of absorption, scattering, and turbulence. This channel may be the traversed distance between a ground station and a satellite or a path of a few kilometers through the atmosphere between two terrestrial transceivers.

The receiver includes a telescope, a filter, a photodetector, an amplifier, a decision device, and a clock recovery unit. The telescope collects the incoming radiation and focuses it onto the filter. The filter removes background radiation and allows only the wavelengths of the signal to pass through it. The photodetector converts the optic radiation into an electronic signal, and the amplifier amplifies the electronic signal. The decision unit determines the nature of the bits of information based on the time of arrival and the amplitude of the pulse. The clock recovery unit operates in parallel to the decision-making unit and synchronizes the data sampling to the decision-making process.

There are three classes of optical material that are commonly used in lenses and windows for OWC systems operating in the mid–far-IR band: semiconductors (single crystal or polycrystalline) silicon and germanium hot-pressed polycrystalline II–IV compound; chemical-vapor-deposited ZnSe and ZnS; and chalcogenide glasses. Silicon and germanium are used for the majority of applications, as their high refractive indices and excellent mechanical strengths and hardnesses simplify optical design.[25–27] An optical wireless receiver for long wavelengths includes in most cases a telescope with special lenses constructed from the materials mentioned above and a high-speed liquid-nitrogen-cooled mercury cadmium telluride detector.[18]

3. Quantum Cascade Lasers: A Brief Review

During the past several years a new generation of lasers, QCLs, has been developed. QCLs are semiconductor laser sources designed for the entire IR wavelength range from 3 to 20 μm. Based on the unipolar nature of the lasing mechanism, QCLs are expected to have excellent direct current modulation, as was recently confirmed in experimental studies that had theoretical limits of several hundred gigahertz.[15,16] This property of QCLs, combined with its favorable transmissivity in the mid-to-long-wavelength IR atmospheric windows, suggests their use in high-capacity free-space communication systems. Recently several QCL operation modes, for example, single mode continuous wave (cw) operation at liquid-nitrogen temperature and pulsed operation mode at and above room temperature, were demonstrated.[17–20] When one considers the operation of a complete OWC system it is important to note that, on the receiver side, longer-wavelength semiconductor detectors (for QCL signal detection) have smaller energy bandgaps. Hence these detectors usually require more cooling because it is easier to generate noise by thermal excitation of the electrons across a small (or narrow) bandgap than a larger one.

4. Mathematical Analysis

In this section we derive a mathematical model for optical signals and noise and determine the signal-to-noise ratio of our OWC communication system. We make two assumptions about the noise: (a) it is defined as additive white Gaussian noise and (b) it is stationary in the time domain.

A. Signal Model

We define the link budget in standard rf communication terminology. The received power at the detector is given by the Friis transmission formula

$$P_S = P_T G_T G_R T_F T_A L_{\mathrm{FS}}, \tag{1}$$

where P_T is the transmitter power, G_T and G_R are the transmitter and receiver telescope gains, respectively, T_F is the optical filter transmissivity, T_A is the atmospheric transmission coefficient, and L_{FS} is the free-space loss. The gain of the transmitter telescope (diffraction limited) is given by

$$G_T \approx \left(\frac{2\pi W_0}{\lambda}\right)^2. \tag{2}$$

Here W_0 is the Gaussian rms width at the transmitter aperture and λ is the transmission wavelength. Similarly, the gain of the receiver telescope is

$$G_R \approx \left(\frac{\pi D_R}{\lambda}\right)^2, \tag{3}$$

where D_R is the receiver aperture diameter. The free-space loss is given by

$$L_{\mathrm{FS}} = \left(\frac{\lambda}{4\pi Z}\right)^2, \tag{4}$$

where Z is the distance between the transmitter and the receiver. The current signal for receiving optical signal P_S is[28]

$$I_1 = \Re P_S + \Re P_{\mathrm{BG}} + I_{\mathrm{DC}}, \tag{5}$$

where R is the detector responsivity, P_{BG} is the background radiation received at the detector, and I_{DC} is the photodiode dark current. Responsivity R is defined by

$$\Re = \eta q \lambda / hc, \tag{6}$$

where q is the electron charge, h is Planck's constant, c is the speed of light, and η is the quantum efficiency of the detector. The received background radiation is calculated by[6]

$$P_{\mathrm{BG}} = A_r \times \mathrm{FOV} \times \Delta\lambda T_F \,\mathrm{Rad} + \frac{2hc^2\alpha \times \mathrm{FOV} \times A_r T_A T_F \Delta\lambda}{\lambda^5[\exp(hc/\lambda KT) - 1]}. \tag{7}$$

The first term in Eq. (7) is related to reflected solar radiation; the second term, to blackbody radiation. A_r is the receiver's effective primary area, FOV is the receiver's field of view; $\Delta\lambda$ is the optical filter's band-

width, Rad is the reflected solar radiance, K is Boltzmann's constant, T is the Earth object blackbody temperature, and α is the factor of radiant absorbance that relates perfect blackbody spectral radiance to the graybody spectral radiance by $(N_\lambda)_{\text{graybody}} = \alpha(N_\lambda)_{\text{blackbody}}$. Note that blackbody radiation can be a troublesome source of noise in IR communication systems. In fact, this radiation can be greater in magnitude than reflected solar radiation in the IR region of the spectrum. Finally, the current signal without any optical signal input is

$$I_0 = \Re P_{\text{BG}} + I_{\text{DC}}. \tag{8}$$

We assume that the background light and dark current can be removed from the signal without any loss of generality such that $I_0 = 0$.

B. Noise Model

The variance in current in the detector that results from background radiation is[2]

$$\sigma_{\text{BG}}{}^2 = 2q\Re P_{\text{BG}}B, \tag{9}$$

where B is the electronic bandwidth. The variance in current in the detector that results from the dark current of the photodiode can be expressed by[29]

$$\sigma_{\text{DC}}{}^2 = 2qI_{\text{DC}}B. \tag{10}$$

Additionally, the variance in current in the detector that results from Johnson (thermal) noise is given by[30]

$$\sigma_{\text{TH}}{}^2 = \frac{4KT_eFB}{R_L}, \tag{11}$$

where R_L is the load resistance, F is the noise figure of the system, and T_e is the equivalent temperature. The detector's current variance caused by laser's relative intensity noise (RIN) in the presence of uniform spectral density is[31]

$$\sigma_{\text{RIN}}{}^2 = (\text{RIN})(\Re P_S)^2B, \tag{12}$$

whereas the current's shot-noise variance in the detector that results from the received signal is[29]

$$\sigma_{\text{ss}}{}^2 = 2q\Re P_SB. \tag{13}$$

From Eqs. (9)–(11), the variance in current noise in the detector element without any signal is given by

$$\sigma_0{}^2 = \sigma_{\text{TH}}{}^2 + \sigma_{\text{DC}}{}^2 + \sigma_{\text{BG}}{}^2, \tag{14}$$

and from Eqs. (9)–(13) the variance in current noise in the detector for receiving an optical signal is given by

$$\sigma_1{}^2 = \sigma_{\text{TH}}{}^2 + \sigma_{\text{DC}}{}^2 + \sigma_{\text{BG}}{}^2 + \sigma_{\text{SS}}{}^2 + \sigma_{\text{RIN}}{}^2. \tag{15}$$

Now we are able to determine our communication system's digital signal-to-noise ratio (DSNR) as[31]

$$\text{DSNR} = \frac{I_1 - I_0}{\sigma_0 + \sigma_1} = \frac{\Re P_S}{\sigma_0 + \sigma_1}. \tag{16}$$

Note that the dominant noise sources in most cases of free-space optic communication are background and thermal noises, both of which can be approximated as Gaussian variables. Hence the cumulative noise can also be approximated as an additive white-noise signal. However, for IR communication systems the noise's probability function has to be precisely identified. For example, at signal levels of a few photons per second, the noise statistics follow a Poisson distribution if all other sources of noise within the receiver are negligible.[1,31,32]

5. Simulation Results and Discussion

We simulated an OWC system's performance within the 0.4–20-μm transmission wavelength region. The simulation was based on moderate-transmission resolution (MODTRAN) computed models integrated with the MATLAB program. MODTRAN is an atmospheric model that was developed at the U.S. Air Force Phillips Laboratory. It can be used to calculate transmission, radiance, or both for a specified path through the atmosphere. For all cases studied we assumed: (a) a U.S. standard atmospheric model, (b) a Mie-generated aerosol phase function, (c) the Sun as the extraterrestrial source; and (d) only single scattering (no multiple scattering). The type of atmospheric path was selected as horizontal, and mode of execution was selected as transmittance. The altitude profiles for temperature, pressure, water vapor, ozone, methane, nitrous oxide, carbon monoxide, and other gases were chosen as defaults. Wind speed and average wind speed were set to zero; the observer height was 100 m, and the remaining parameters were fixed as defaults.

Experiments[23,24] with optical wireless communication systems indicated that, on average, scintillation fade owing to air turbulence at wavelengths of 780 and 810 nm for 1 km was of the order of 4–5 dB. These small values of scintillation fading, rather than tens of decibels as a result of aerosol attenuation, show that scintillation does not substantially affect link availability.[9] Therefore the use of MODTRAN software, which does not simulate turbulence scintillation, is appropriate for studying link availability.

Our approach to evaluating link availability is to calculate the signal power, the background power, the detector noise, and the DSNR performance parameter as a function of transmission wavelength for all weather conditions. The simulation calculations were performed for several standard international visibility code weather conditions and precipitation[9]: very clear weather (50-km visibility); clear weather (18.1-km visibility) with drizzle at a 0.25-mm/h rate; light haze (5.9-km visibility) with light rain at a 2.5-mm/h rate; haze (2.8-km visibility) with medium rain at a 12.5-mm/h rate; thin fog (1.9-km visibility) with heavy rain at 25 mm/h; light fog (770-m visibility) with cloudbursts of 100 mm/h; and thick (200-m visibility) and dense (50-m visibility) fog without rain.

First we calculated the total atmospheric attenuation (in units of decibels per kilometer) as a function of the visibility conditions. These conditions can be

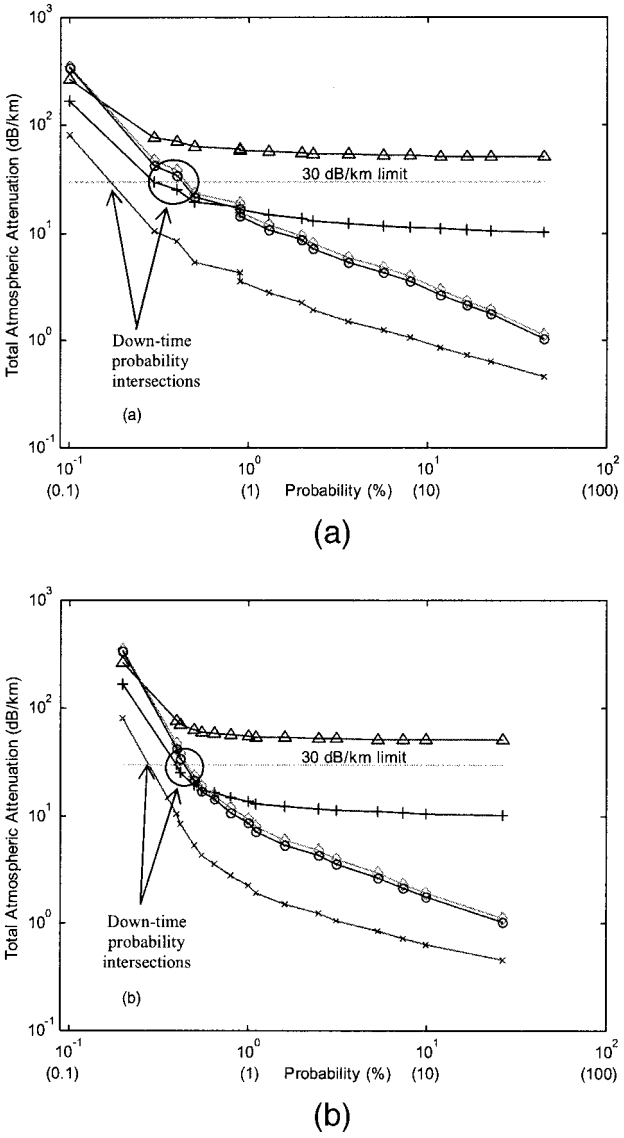

Fig. 3. (a) Total New York City atmospheric attenuation versus percentage of frequency of visibility from hourly observations for specified transmission wavelengths: 0.785 μm (circles), 1.55 μm (diamonds), 7 μm (triangles), 10 μm (×'s) and 20 μm (+'s). (b) Total San Francisco atmospheric attenuation versus percentage of frequency of visibility from hourly observations for specified transmission wavelengths: 0.785 μm (circles), 1.55 μm (diamonds), 7 μm (triangles), 10 μm (×'s) and 20 μm (+'s).

represented by percentage data of the frequency of visibility from hourly observations, which are available for most airports in the world. The results of these calculations are shown in Fig. 3 for New York City [Fig. 3(a)] and for San Francisco [Fig. 3(b)], with better visibility conditions in the latter case. We compared the derived attenuations for transmission wavelengths of 0.785, 1.55, 7, 10, and 20 μm. For all visibility conditions, the 7-μm wavelength provided the highest loss level (above 50 dB/km), whereas the lowest loss level was provided by the 10-μm wavelength. The 30-dB/km limit line indicates the ability of available OWC systems to compensate for atmospheric loss. System downtime was determined by the intersection of this line with the specific wavelength curve. Downtimes of approximately 0.2–0.4% (in both cities) were obtained for almost all wavelengths (except for the 7-μm wavelength) for a 1-km communication distance. The 10-μm wavelength introduced a system availability improvement of ~0.2% (from 99.6% to 99.8%) compared with the availabilities at 0.785- and 1.55-μm wavelengths. For the 7-μm wavelength, which lies within an atmospheric absorption window, there was no intersection between its curve and the limit line. This indicates that no present OWC system can operate properly at this wavelength.

Figure 4 depicts the normalized transmission determined by a receiver-generated current (in amperes per watt of transmission power) for various weather conditions. The calculated transmission was normalized for a 1-km atmospheric path with detector quantum efficiency, transmitter and receiver gains, optical filter transmissivity, and free-space loss parameters all set to value 1. Given a different parameter value, we can conveniently multiply it by the normalized transmission to get a relevant result. The normalized transmission for very clear weather is given in Fig. 4(a), from which we can see that the preferable transmission wavelengths are within the 9–13 μm long-wave IR band. This dependence of transmission on wavelength corresponds to major IR absorption windows in which transmission through the atmosphere is essentially negligible. Similar wavelength dependence was obtained for normalized transmission for clear weather with drizzle (0.25 mm/h), light haze with light rain (2.5 mm/h), and haze with medium rain (12.5 mm/h), as shown in Figs. 4(b), 4(c), and 4(d), respectively. Obviously, the detector current is reduced for all wavelengths when visibility is degraded. Figures 4(e)–4(h) depict normalized transmission for foggy weather. In Fig. 4(e) the normalized transmission is shown for thin fog with heavy rain (25 mm/h), where preferred transmission wavelengths are again within the 9–13-μm band and transmission in the visible and short-wave IR bands is well reduced. Similar wavelength dependence was observed in more foggy weather conditions, as illustrated in Fig. 4(f) for light fog with cloudburst (100 mm/h). Again, as the visibility ranges become smaller, the generated current is decreased. For thick fog [Fig. 4(g)] and dense fog [Fig. 4(h)], the peak current was nearly 10^{-1} and 10^{-7} A/W, respectively, at 11-μm transmission wavelength, whereas transmission through the atmosphere for wavelengths below 8 μm was essentially reduced. Note that, in the long-IR 8–13-μm band, better transmission was obtained in thick fog (without rain) than in light fog (with cloudburst), although the visibility was degraded in the former case. This result underscores the dependence of free-space transmittance on extreme rain. It is clear that, for all the cases studied, the preferred transmission wavelengths were within the 9–13-μm band, with even better transmissivity near 11 μm.

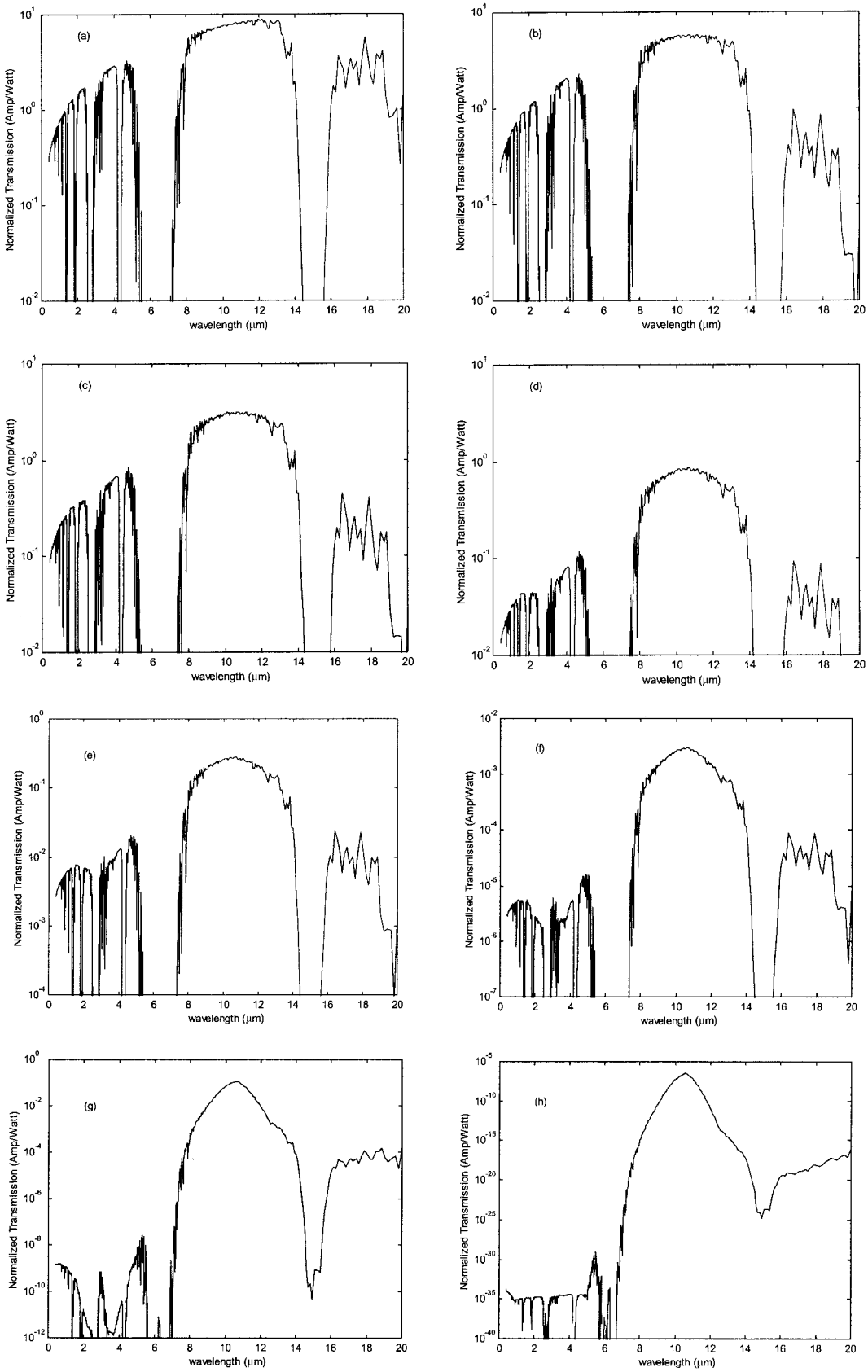

Fig. 4. Normalized transmission (A/W) versus wavelength for several weather conditions: (a) very clear weather (visibility, 50 km), (b) clear weather (visibility, 18.1 km) with drizzle at a 0.25-mm/h rate, (c) light haze (visibility, 5.9 km) with light rain at 2.5 mm/h, (d) haze (visibility, 2.8 km) with medium rain at 12.5 mm/h, (e) thin fog (visibility, 1.9 km) with heavy rain at 25 mm/h, (f) light fog (visibility, 770 m) with cloudburst at 100 mm/h, (g) thick fog (visibility, 200 m) without rain, and (h) dense fog (visibility, 50 m) without rain.

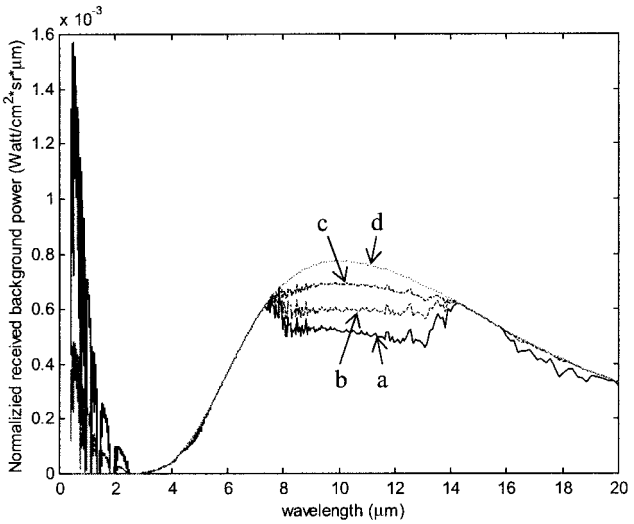

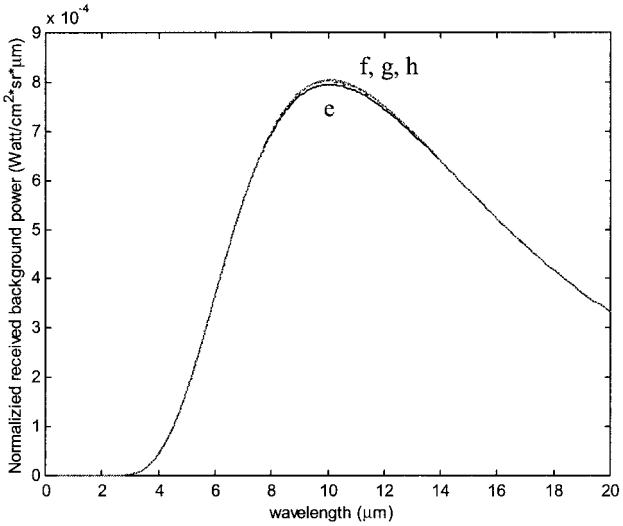

Fig. 5. Normalized received background power ($P_{BG}/A_r \times FOV \times \Delta\lambda T_F$) versus transmission wavelength for all weather conditions defined in Fig. 4.

Thus far we have analyzed the wavelength dependence of total atmospheric attenuation of an OWC system that is free from the effects of internal or external noise. Obviously, these effects must be considered when we deal with a real OWC system. The external noise effect is related to the received background radiation P_{BG}, which we determined mathematically in Section 4 of this paper. Figure 5 depicts the dependence on wavelength of the normalized received background power $P_{BG}/A_r \times FOV \times \Delta\lambda T_F$ for all defined weather conditions. A Sun elevation angle of 60° and typical 300-K Earth object blackbody temperature were assumed. We can see that for almost all weather conditions (except for clear weather) the dominant background radiation levels lie within the 7–15-μm wavelength band with higher levels calculated under hazy and foggy conditions (curves a–h). In this band the atmospheric background consists primarily of thermal emissions by atmospheric gases and particles. For clear weather conditions (curves a and b) the dominant background radiation level lies within the visible and short-IR bands, where the atmospheric background consists primarily of scattered solar radiation. The dependence of background radiation on wavelength as described significantly affects OWC system performance, as we discuss what follows.

Table 1. System Model Inputs

Quantity	Symbol	Value	Unit
Peak power	P_T	1	W
Transmitter–receiver distance	Z	1	km
Gaussian transmitter aperture width (rms)	W_0	1	mm
Optical filter transmissivity	T_F	0.5	
Earth object blackbody temperature	T	300	K
Radiant absorptance factor	α	0.5	
Filter optical bandwidth	$\Delta\lambda$	10	nm
Receiver aperture diameter	D_R	10	cm
P–I–N quantum efficiency	η	0.8	
Detector electronic bandwidth	B	1	GHz
Load resistance	R_L	100	Ω
Circuit noise figure	F	4	
Equivalent temperature	Te	290	K

In the last part of the simulation, the system's performance as determined by the DSNR of the system was analyzed. Table 1 lists all the pertinent physical parameters that we used as input to the system model. The given values are typical for existing laser sources within the specified wavelength region and for a commercially fast liquid-nitrogen-cooled HgCdTe detector.[27] The wavelength dependence of free-space loss and receiver and transmitter gains for a diffraction-limited system [formulas (2)–(4)] are also considered. As mentioned above, in free-space optic communication the dominant noise sources are mostly background and thermal noises. Therefore we analyze system performance in terms of these types of noise.

The DSNR of a background-noise-limited system is shown in Fig. 6 for all weather conditions. The DSNR values presented are −20 to 100 dB. Although the 0-dB bound is considered to be the lowest bound for receiver signal detecting, negative values to −20 dB are also shown. For a much shorter (less than 1-km) path link these low values become positive, thus providing reliable system performance. A DSNR of 100 dB, however, corresponds to an extremely high level of system performance, and therefore higher levels are omitted from the figure. The highest DSNR levels were obtained in the visible and short-IR bands for all cases. These results were expected because of the dependence on wavelength of the background radiation (as described above). However, in the 7–15-μm band, system performance was significantly reduced by the presence of high levels of background radiation. For clear weather conditions (curves a and b), the advantage of the visible and short-IR bands was less dominant be-

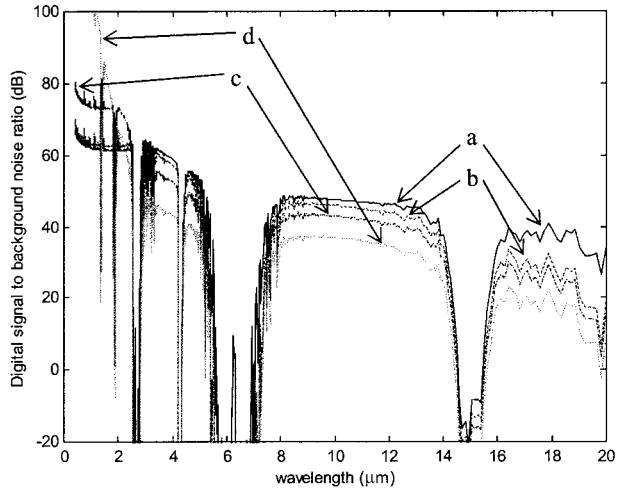

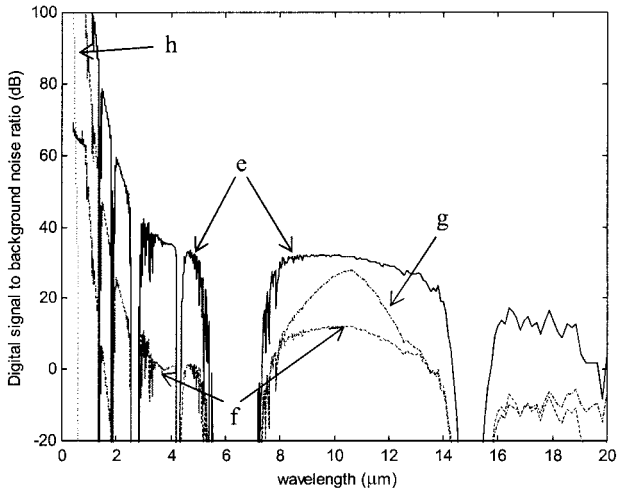

Fig. 6. DSNR of background-noise-limited system [$\mathrm{DSNR_{BG}} = (\mathrm{RP_S})/(2\sigma_{\mathrm{BG}})$] versus transmission wavelength for all weather conditions defined in Fig. 4.

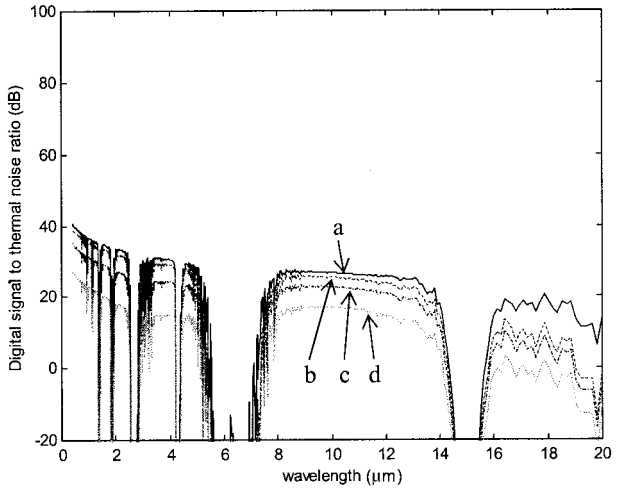

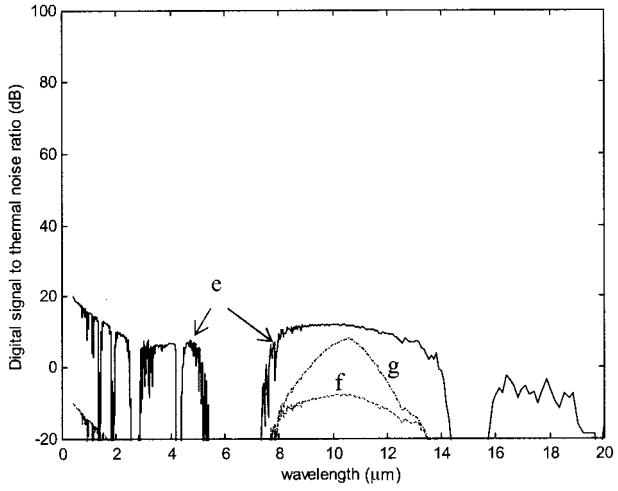

Fig. 7. DSNR of thermal-noise-limited system [$\mathrm{DSNR_{TH}} = (RP_S)/(2\sigma_{\mathrm{TH}})$] versus transmission wavelength for all weather conditions defined in Fig. 4.

cause of the high background radiation levels that were present in these bands. In the 7–15-μm band, the highest DSNR levels (more than 45 dB) were obtained for clear weather conditions (curves a and b), whereas in the 0.4–3-μm band the highest DSNR levels (75 dB and higher, except for low DSNRs within the atmospheric absorption windows) were obtained for hazy weather (curves c and d). Similar wavelength dependence was observed for thin, light, and thick foggy weather conditions (curves e, f, and g) with DSNR penalties of approximately 10, 20, and 50 dB, respectively, in the visible and short-IR bands. However, in the long-IR 8–13-μm band an improvement of 16 dB in system performance was obtained in thick fog (without rain) from that in light fog (with cloudburst), corresponding to the normalized transmission as described above. For dense fog (curve h), poor system performance was observed for almost the entire spectrum. The allowable transmission wavelengths in this case lie within the 0.4–0.7-μm visible band.

Figure 7 depicts the DSNR of our thermal-noise-limited system when thermal noise is the dominant system noise source for all weather conditions. We can see that the highest DSNR levels (approximately 25 dB and above) were observed for clear weather conditions (curves a and b). Obviously, the advantage of visible and short-IR bands shown in the background-noise-limited system no longer exists, which results in similar DSNR levels with differences of as much as 15 dB for the entire atmospheric transmission spectrum (except for low DSNRs within the atmospheric absorption windows). For thin fog (curve e) these differences were reduced to ~5 dB only, indicating that the system still favored the visible and short-IR bands over the long-IR band. However, for light and thick fog (curves f and g, respectively) the long-IR 8–13-μm band was the preferable transmission band, with DSNR improvements of ~5 and ~50 dB, respectively. Finally, for dense fog (curve h) the highest DSNR levels (as much as −47 dB and below, and therefore not shown in the

figure) were observed within the long-IR 8–13-μm wavelength band.

6. Conclusions

We analyzed the wavelength dependence of a short-distance terrestrial data link performance, using visible through long-IR transmission wavelengths. A mathematical model for the link performance parameters was derived. Using this model, we performed a simulation of our system for several weather conditions. It is easy to see that long wavelengths are advantageous only when there are mid-attenuation events. At low- and high-attenuation events, performance is identical. Therefore link availability at the far IR is improved only during mid-attenuation events.

For total atmospheric attenuation calculations the preferable transmission wavelength for all visibility conditions was 10 μm, corresponding to ~99.8% system availability, with improvement of ~0.2% compared with values for 0.785- and 1.55-μm wavelengths. These results were obtained for two U.S. cities at a communication distance of 1 km. An improvement of 0.2% for link availability achieved by the longer wavelengths should be considered with respect to complexity and cost of quantum cascade laser transmitters and far-IR receivers that include liquid-nitrogen-cooled mercury cadmium telluride detectors.[33]

Advanced normalized transmission calculations showed that in clear, hazy, and thin to light fog weather conditions the preferable transmission wavelengths were within the 9–13-μm long-wave IR band. However, for thick to dense fog weather conditions, a (low-value) maximum generated current was obtained near the 11-μm wavelength. For all the cases studied, the preferred transmission wavelengths were within the 9–13-μm band, with even better transmissivity near the 11-μm wavelength. Therefore the use of a QCL as a unique long-wave IR laser source is essential.

We analyzed the performance of a system as determined by its DSNR by taking into account the dominant noise sources. For a background-noise-limited system the best performance was obtained within the 0.4–0.7-μm visible band, owing to its much lower background radiation level than that of the 7–15-μm wavelength band. For a thermal-noise-limited system in clear, hazy, and thin to light foggy weather conditions, however, similar system performance was observed for the entire spectrum, whereas in thick to dense foggy weather conditions better system performance was obtained within the 8–13-μm long-wave IR band. The advantage of longer IR wavelengths relative to shorter wavelengths in dense fog weather conditions for a 200-m terrestrial link path was evaluated in a recent experiment[28] in which clearly better performance of a 8.1-μm QCL compared with a 0.85 μm near-IR laser was reported. All these results underscore the dependence of free-space transmission on dense fog.

The influence of atmospheric turbulence on link performance lessens at longer wavelengths.[21] But, as we already mentioned, experiments[23,24] with optical wireless communication systems have shown that scintillation does not substantially affect link availability.[9] Moreover, if the system is designed with a multiple transmitter and wide receiver aperture scintillation, fading is reduced even further.[23] Therefore we can conclude that the effect of turbulence on link availability is negligible.

In the studies reported in this paper, all the calculations were performed for a 1-km terrestrial link path. Obviously, for a longer-distance OWC link, system performance worsens. Therefore future studies should concentrate on advanced adaptive methods or hybrid OWC–rf systems that operate properly under such conditions. Obviously, the choice of OWC operation wavelength should take eye-safety requirements into consideration.

The authors are grateful for the support of the Israeli–German DIP research fund and to the Ontar Corporation for allowing us to use its PcModWin4.0 software for research calculations.

References

1. R. M. Gagliardi and S. Karp, *Optical Communication*, 2nd ed. (Wiley, New York, 1995).
2. S. G. Lambert and W. L. Casey, *Laser Communication in Space* (Artech House, Boston, Mass., 1995).
3. S. Arnon, "Optical wireless communication," in *Encyclopedia of Optical Engineering*, R. G. Driggers, ed. (Marcel Dekker, New York, to be published).
4. B. R. Strickland, M. J. Lavan, E. Woodbridge, and V. Chan, "Effects of fog on the bit-error rate of a free-space laser communication system," Appl. Opt. **38,** 424–431 (1999).
5. W. R. Leeb, "Degradation of signal to noise ratio in optical free-space data links due to background illumination," Appl. Opt. **28,** 3443–3449 (1989).
6. N. S. Kopeika and J. Bordogna, "Background noise in optical communication systems," Proc. IEEE **58,** 1571–1577 (1970).
7. N. S. Kopeika, "General wavelength dependence of imaging through the atmosphere," Appl. Opt. **20,** 1532–1536 (1981).
8. I. I. Kim, B. McArthur, and E. Korevaar, "Comparison of laser beam propagation at 785 nm and 1550 nm in fog and haze for optical wireless communications," in *Optical Wireless Communications III*, E. Korevaar, ed., Proc. SPIE **4214,** 26–37 (2001).
9. I. I. Kim and E. Korevaar, "Availability of free-space optics (FSO) and hybrid FSO/RF systems," in *Optical Wireless Communications IV*, E. Korevaar, ed., Proc. SPIE **4530,** 84–95 (2001).
10. E. J. McCartney, *Optics of the Atmosphere* (Wiley, New York, 1976).
11. National Weather Service, *International Station Meteorological Climate Summary, V. 4.0* (Federal Climate Complex, Asheville, N.C., 1996).
12. M. R. Clay and A. P. Lenham, "Transmission of electromagnetic radiation in fogs in the 0.53–10.1-μm wavelength range," Appl. Opt. **20,** 3831–3832 (1981).
13. T. S. Chu and D. C. Hogg, "Effects of precipitation on propagation at 0.63, 3.5, and 10.6 microns," Bell Syst. Tech. J. **47,** 723–759 (1968).
14. P. Christopher, "Worldwide infrared and millimeter wave satellite performance," in *Free-Space Laser Communication Technologies XIII*, G. S. Mecherler, ed., Proc. SPIE **4272,** 268–281 (2001).
15. F. Capasso, C. Gmachi, R. Paiella, A. Tredicucci, A. L.

Hutchinson, D. L. Sivco, J. N. Baillargeon, A. Y. Cho, and H. C. Liu, "New frontiers in quantum cascade lasers and applications," IEEE J. Sel. Top. Quantum Electron. **6,** 931–947 (2000).
16. R. Martini, C. Gmachi, J. Falciglia, F. G. Curti, C. G. Bethea, F. Capasso, E. A. Whittaker, R. Paiella, A. Tredicucci, A. L. Hutchinson, D. L. Sivco, and A. Y. Cho, "High speed modulation and free-space optical audio/video transmission using quantum cascade lasers," Electron. Lett. **37,** 191–193 (2001).
17. R. Martini, C. Bethea, F. Capasso, C. Gmachl, R. Paiella, E. A. Whittaker, H. Y. Hwang, D. L. Sivco, J. N. Baillargeon, and A. Y. Cho, "Free-space optical transmission of multimedia satellite data streams using mid-infrared quantum cascade lasers," Electron. Lett. **38,** 181–183 (2002).
18. R. Martini, C. Gmachi, A. Tredicucci, F. Capasso, A. L. Hutchinson, D. L. Sivco, and A. Y. Cho, "High duty cycle operation of quantum cascade lasers based on graded superlattice active regions," J. Appl. Phys. **89,** 7735–7738 (2001).
19. S. Blaser, D. Hofstetter, M. Beck, and J. Faist, "Free-space optical data link using a Peltier-cooled quantum cascade laser," Electron. Lett. **37,** 778–780 (2001).
20. F. Capasso, R. Paiella, R. Martini, R. Colombelli, C. Gmachi, T. L. Myers, M. S. Taubman, R. M. Williams, C. G. Bethea, K. Unterrainer, H. Y. Hwang, D. L. Sivco, A. Y. Cho, A. M. Sergent, H. C. Liu, and E. A. Whittaker, "Quantum cascade lasers: ultrahigh-speed operation, optical wireless communication, narrow linewidth, and far-infrared emission," IEEE J. Quantum Electron. **38,** 511–532 (2002).
21. L. C. Andrews and R. L. Philips, *Laser Beam Propagation through Random Media* (SPIE Optical Engineering Press, Bellingham, Wash., 1998).
22. S. Arnon, "The effects of atmospheric turbulence and building sway on optical wireless communication systems," Opt. Lett. **28,** 129–131 (2003).
23. I. Kim, R. Stieger, J. Koontz, C. Moursund, M. Barclay, P. Adhikari, J. Schuster, E. Korevaar, R. Ruigrok, and C. DeCusatis, "Wireless optical transmission of fast Ethernet, FDDI, ATM, and ESCON protocol data using the TerraLink laser communication system," Opt. Eng. **37,** 3143–3155 (1998).
24. B. R. Strickland, M. J. Lavan, E. Woodbridge, and V. Chan, "Effects of fog on the bit error rate of a free-space laser communication system," Appl. Opt. **38,** 424–434 (1999).
25. J. M. Lloyd, *Thermal Imaging Systems* (Plenum, New York, 1975).
26. P. R. Norton, "Infrared image sensors," Opt. Eng. **30,** 1649–1663 (1991).
27. W. Wolfe, "Electro-optical components," in *The Infrared & Electro-Optical System Handbook*, W. D. Rogatto, ed. (SPIE Optical Engineering Press, Bellingham, Wash., 1993), Vol. 3, chap. 1, p. 1.
28. S. Arnon and N. S. Kopeika, "Laser satellite communication networks—vibration effects and possible solutions," Proc. IEEE **85,** 1646–1661 (1997).
29. N. S. Kopeika, *A System Engineering Approach to Imaging* (SPIE Optical Engineering Press, Bellingham, Wash., 1998).
30. A. Yariv, *Optical Electronics*, 4th ed., (Holt, Rinehart & Winston, New York, 1991), pp. 241–244 and 355–460.
31. L. Kazovsky, S. Benedetto, and A. Willner, *Optical Fiber Communication Systems* (Artech House, Boston, Mass., 1991), p. 223.
32. A. Papoulis, *Probability, Random Variables and Stochastic Processes*, 3rd ed. (McGraw-Hill, New York, 1991).
33. E. Korevaar, I. Kim, and B. McArthur, "Debunking the recurring myth of a magic wavelength for free-space optics," in *Optical Wireless Communications V*, E. J. Korevaar, ed. Proc. SPIE **4873,** 155 (2002).